Journal of the Optical Society of Korea
Vol. 20, No. 6, December 2016, pp. 663-668

ISSN: 1226-4776(Print) / ISSN: 2093-6885(Online)
DOI: https://doi.org/10.3807/JOSK.2016.20.6.663

A Numerical Study of Different Types of Collimators for a High-Resolution Preclinical CdTe Pixelated Semiconductor SPECT System

Hyun-Woo Jeong[1], Jong Seok Kim[2], Se Young Bae[2], Kanghyen Seo[2], Seung Hun Kim[2], Seong Hyeon Kang[2], Dong Jin Shin[2], Chang-Lae Lee[3], Kyuseok Kim[3], and Youngjin Lee[2]*

[1]Department of Biomedical Engineering and School of Medicine, Eulji University, Gyeonggi-do 13135, Korea
[2]Department of Radiological Science, Eulji University, Gyeonggi-do 13135, Korea
[3]Department of Radiological Science, Yonsei University, Wonju 26493, Korea

(Received September 30, 2016 : revised November 28, 2016 : accepted November 30, 2016)

In single-photon-emission computed tomography (SPECT) with a pixelated semiconductor detector (PSD), not only pinhole collimators but also parallel-hole collimators are often used in preclinical nuclear-medicine imaging systems. The purpose of this study was to evaluate and compare pinhole and parallel-hole collimators in a PSD. For that purpose, we paired a PID 350 (Ajat Oy Ltd., Finland) CdTe PSD with each of the four collimators most frequently used in preclinical nuclear medicine: (1) a pinhole collimator, and (2) low-energy high-resolution (LEHR), (3) low-energy general-purpose (LEGP), and (4) low-energy high-sensitivity (LEHS) parallel-hole collimators. The sensitivity and spatial resolution of each collimator was evaluated using a point source and a hot-rod phantom. The highest sensitivity was achieved using LEHS, followed by LEGP, LEHR, and pinhole. Also, at a source-to-collimator distance of 2 cm, the spatial resolution was 1.63, 2.05, 2.79, and 3.45 mm using pinhole, LEHR, LEGP, and LEHS, respectively. The reconstructed hot-rod phantom images showed that the pinhole collimator and the LEHR parallel-hole collimator give a fine spatial resolution for preclinical SPECT with PSD. In conclusion, we successfully compared different types of collimators for a preclinical pixelated semiconductor SPECT system.

Keywords : Gamma ray, Photon detection, Medical application, Photodetectors
OCIS codes : (040.5160) Photodetectors; (040.6040) Silicon; (060.0060) Fiber optics and optical communications; (060.4510) Optical communications

I. INTRODUCTION

A conventional single-photon-emission computed tomography (SPECT) system is most often based on the Anger camera principle, using a collimator in front of a NaI(Tl) or CsI(Tl) scintillation crystal [1]. However, the intrinsic resolution of a scintillation detector is relatively low (approximately 3.0-4.0 mm full width at half maximum (FWHM)) [2]. One strategy to cope with this low intrinsic resolution is to use a pixelated semiconductor detector (PSD) employing cadmium telluride (CdTe) or cadmium zinc telluride (CZT) [3-7]. The intrinsic resolution of a PSD is almost equal to the pixel size, because the carriers are collected individually for each pixel, with direct conversion of gamma-ray photons into electrons [4].

In SPECT, the collimator is an essential component of the system, because the imaging performance (including sensitivity and spatial resolution) depends mainly on the collimator [8]. Collimators types are generally classified as parallel-hole, pinhole, converging, and diverging. Almost all preclinical SPECT is performed with a pinhole or a parallel-hole collimator. The pinhole collimator has been widely used for preclinical SPECT systems because of its excellent spatial resolution [9-11]. A pinhole collimator can be very useful in preclinical research where a small organ, such as the thyroid or parathyroid gland, is imaged [12, 13]. Also, nearly all preclinical SPECT systems use a parallel-hole collimator as the image-forming

*Corresponding author: radioyoungj@gmail.com
Color versions of one or more of the figures in this paper are available online.

aperture. Parallel-hole collimators are generally desirable for almost all imaging applications in nuclear medicine, due to the optimal image performance offered by such a dense arrangement of apertures. Although we need to select a collimator to obtain appropriate image performance and accurate analysis results, there have been no comparative studies on image performance with various collimators in preclinical pixelated semiconductor SPECT systems. Therefore, in this study we compared the imaging performance of a pinhole and three types of parallel-hole collimators (low-energy high-resolution (LEHR), low-energy general-purpose (LEGP), and low-energy high-sensitivity (LEHS)) in a preclinical pixelated semiconductor SPECT system, using a GEANT4 Application for Tomographic Emission (GATE) simulation.

The collimators were simulated with a PID 350 (Ajat Oy Ltd., Finland) CdTe PSD using a GATE. The sensitivity and spatial resolution were evaluated for each source-to-collimator distance. To evaluate the overall imaging performance, a hot-rod phantom was designed using GATE. The simulated comparison results obtained for various collimators are presented and discussed.

II. METHODS

2.1. Monte Carlo simulation

Monte Carlo simulation, a statistical technique using random processes, is a crucial tool in studying the effects of various system parameters and components in the field of nuclear medicine. GATE is a widely used Monte Carlo simulation platform, with general-purpose code Geant4 and advanced open-source software developed by the international OpenGATE collaboration in 2001 [14]. The accuracy, usefulness, and effectiveness of this platform have been confirmed in many studies [14-17]. In this study, we used GATE version 6.

2.2. PID 350 CdTe PSD

Among available semiconductor detectors, those with a single chemical element, such as silicon (Si) or germanium (Ge), are most frequently used in nuclear medicine [18,19]. However, the low atomic number of Si leads to low absorption efficiency, due to low stopping power for high-energy gamma-ray photons, and Ge has major limitations, such as a narrow band-gap energy which is useful only at cryogenic temperatures [20, 21]. Consequently, many nuclear- medicine studies have used pixelated semiconductor materials with wide band gaps, such as CdTe. CdTe pixelated semiconductor materials have been studied for their applications in nuclear-medicine imaging. The useful properties of CdTe include its wide band gap, high atomic number, and good charge transport [22-24].

We modeled the PID 350 CdTe PSD geometry using the tool within GATE. The pixel size of the PID 350 CdTe PSD was 0.35 × 0.35 mm^2, with an array of 128 × 128 pixels. The detector thickness was 1 mm, and the physical gap was 1 pixel. The CdTe PSD had 32% efficiency at a gamma-ray energy of 140 keV (wavelength 10^{-12} m).

2.3. Pinhole and Three Parallel-hole Collimators

In gamma-ray imaging, collimators play an important role in imaging performance, including spatial resolution and sensitivity. To determine spatial resolution and sensitivity, we should consider a collimator's physical parameters: hole diameter, length, and septal thickness. Figure 1 shows a schematic diagram of collimator geometry. As collimator hole diameter and hole length increase, we realize high sensitivity but low spatial resolution. Also, as septal thickness and septal length increase, high spatial resolution can be obtained through the narrow point-spread function (PSF) or line-spread function (LSF).

We designed four preclinical collimators: pinhole, LEHR parallel-hole, LEGP parallel-hole, and LEHS parallel-hole. A previous paper demonstrated that the reconstructed hot-rod phantom images employing the most frequently used collimator

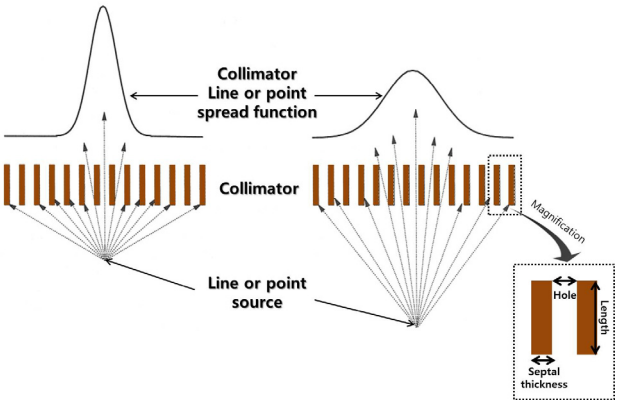

FIG. 1. Schematic diagram of collimator geometry, including physical parameters such as collimator hole diameter, length, and septal thickness.

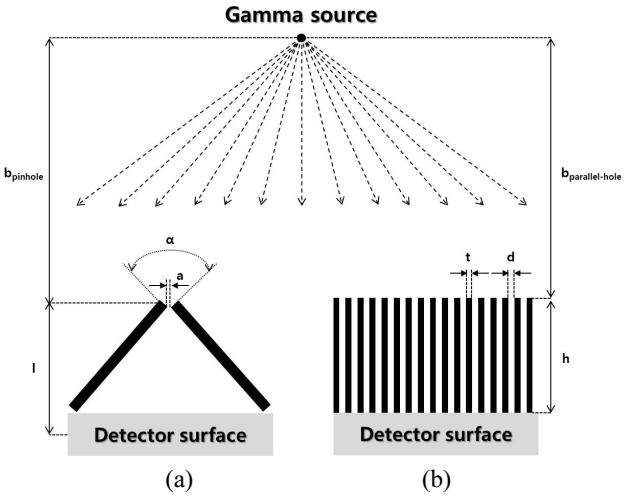

FIG. 2. Schematic descriptions of (a) pinhole and (b) parallel-hole collimators.

materials (lead, tungsten, gold, and depleted uranium) were difficult to distinguish accurately [5]. Based on this result, tungsten offers a spatial resolution similar to those of the much more expensive gold and depleted uranium, so we considered a tungsten collimator in this study. Figure 2 shows the cross-sectional views for the pinhole and parallel-hole collimators.

In a pinhole collimator system, the efficiency $\varepsilon_{pinhole}$ and resolution $R_{pinhole}$ of the collimator were defined as follows [12]:

$$\varepsilon_{pinhole} = \frac{a_{effective_{efficiency}}{}^2 cos^3\theta}{16 b_{pinhole}{}^2} \left(a_{effective_{efficiency}} = \sqrt{a\left[a + \frac{2}{\mu} tan\left(\frac{\alpha}{2}\right)\right]}\right) \quad (1)$$

$$R_{pinhole} = \frac{a_{effective_{resolution}}(l + b_{pinhole})}{l} \left(a_{effective_{resolution}} = a + \frac{ln\,(2)}{\mu} tan\left(\frac{\alpha}{2}\right)\right) \quad (2)$$

where $a_{effective_{efficiency}}$ is the effective pinhole diameter for sensitivity, θ is the angle between the source and detector center lines, $b_{pinhole}$ is the source-to-pinhole collimator distance, a is the pinhole diameter, μ is the linear attenuation coefficient, α is the aperture angle of the collimator, $a_{effective_{resolution}}$ is the effective pinhole diameter for resolution, and l is the distance from the pinhole aperture to the detector surface. We designed the pinhole collimator using a GATE simulation. The aperture angle was 50°, and the pinhole was 1.2 mm in diameter. In this study the magnification factor of the pinhole collimator was 3.0, due to the ratios of the distances among source, collimator, and detector.

In a parallel-hole collimator system, the efficiency ε_{-hole} and resolution R_{-hole} of the collimator were defined as follows [2, 8]:

$$\varepsilon_{-hole} = K^2 \left(\frac{d}{h_{effective}}\right)^2 \frac{d^2}{(d+t)^2} \left(h_{effective} = h - 2\mu^{-1}\right) \quad (3)$$

$$R_{-hole} = d\,\frac{h_{effective} + b_{-hole}}{h_{effective}} \quad (4)$$

where K is a constant that depends on the hole shape, d is the hole diameter, t is the septal thickness, $h_{effective}$ is the effective length of the collimator, h is the length of the collimator, and b_{-hole} is the source-to-collimator distance. We designed the three types of parallel-hole collimators (LEHR, LEGP, and LEHS parallel-hole collimators) also using GATE simulations. The specifications of these parallel-hole collimators are shown in Table 1.

TABLE 1. Specifications of the parallel-hole collimators

	LEHR	LEGP	LEHS
Hole diameter (mm)	1.2	1.6	2
Length (mm)	30	25.4	25.4
Septal thickness (mm)	0.2	0.25	0.3

2.4. Evaluation of Imaging Performance

To compare and evaluate the performance of the gamma-camera systems, we evaluated both sensitivity and spatial resolution. We used a ^{99m}Tc point source with an activity of 1 MBq, with a 900-second scan time. Energy discrimination was applied to the 20% symmetrical energy window. The number of projections was 90 over 360°, and the data acquisition time was 10 seconds per view. Images were reconstructed using the ordered subsets-expectation maximization (OSEM) method. We used four subsets with five iterations. The evaluated sensitivity was represented in counts per second per kBq (cps/kBq). Spatial resolution was represented by the FWHM, using a PSF in air.

To reduce statistical errors, ten simulations were performed for each source-to-collimator distance. The standard deviation σ was calculated as follows:

$$\sigma = \sqrt{\frac{\sum_{i=1}^{n}\left(N_i - \acute{N}\right)^2}{(n-1)}} \quad (5)$$

where n is the number of measurements taken (here 10), N_i is the datum from each measurement, and $\acute{N}$ is the average of the data.

Finally, to evaluate overall imaging performance, hot-rod phantom images were generated in a GATE simulation, consisting of seven areas with rods of varying diameters that could be filled with activity. This phantom was filled with a water solution of ^{99m}Tc. Figure 3 shows the hot-rod phantom diagram.

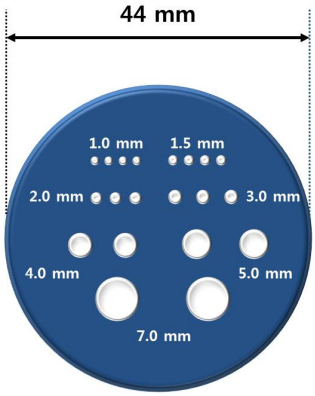

FIG. 3. Hot-rod phantom diagram. This phantom consisted of seven areas with rods of varying diameters (1.0, 1.5, 2.0, 3.0, 4.0, 5.0, and 7.0 mm) that can be filled with activity. Activities were 30, 55, 90, 135, 180, 280, and 445 kBq, respectively.

The distances between the point source or hot-rod phantom and collimator were 1, 2, 3, 4, and 5 cm for preclinical imaging.

III. RESULTS AND DISCUSSION

The sensitivity of the parallel-hole collimator is independent of the distance of the object from the collimator, in all cases. The average sensitivities for each source-to-collimator distance and collimator are shown in Fig. 4. A comparison of the sensitivities of the four types of collimators is shown in Fig. 5. The average sensitivities for the LEHR, LEGP, and LEHS parallel-hole collimators are 0.09247, 0.23441, and 0.36773 cps/kBq respectively. Meanwhile, the sensitivity for the pinhole collimator at a source-to-collimator distance of 2 cm is 0.00393 cps/kBq. In increasing order, the sensitivity rises from pinhole to LEHR parallel-hole to LEGP parallel-hole to LEHS parallel-hole collimator. When we compare the LEHS parallel-hole collimator to the others, the sensitivity of the LEHS is respectively 3.98, 1.57, and 93.57 times as high as that of the LEHR, LEGP, and pinhole collimators.

The spatial resolutions of the parallel-hole collimators decrease with increasing distance from the collimator; thus the spatial resolution will be best when the object is closest to the parallel-hole collimator, in all cases. The average spatial resolution for each source-to-collimator distance and collimator is shown in Fig. 6. A comparison of the spatial resolution with respect to the four types of collimators is shown in Fig. 7. At a source-to-collimator distance of 2 cm, the spatial resolution increases in order from pinhole to LEHR to LEGP to LEHS parallel-hole collimator. According to these results, the average spatial resolution using the pinhole collimator was respectively 20.49, 41.58, and 52.75% better than with LEHR, LEGP, and LEHS parallel-hole collimators. In our system, the spatial resolution of images with either pinhole

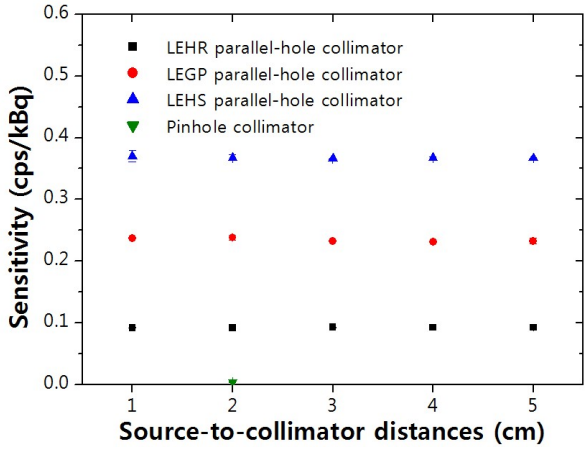

FIG. 4. Simulation results for the sensitivity with respect to the source-to-collimator distance, for a pinhole collimator and three parallel-hole collimators.

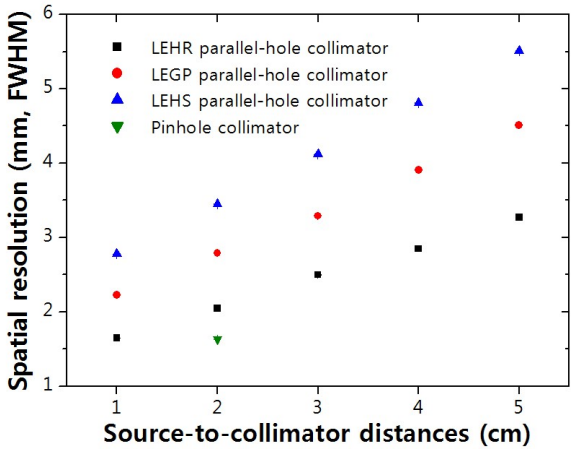

FIG. 6. Simulation results for the spatial resolution with respect to the source-to-collimator distance, for a pinhole collimator and three parallel-hole collimators.

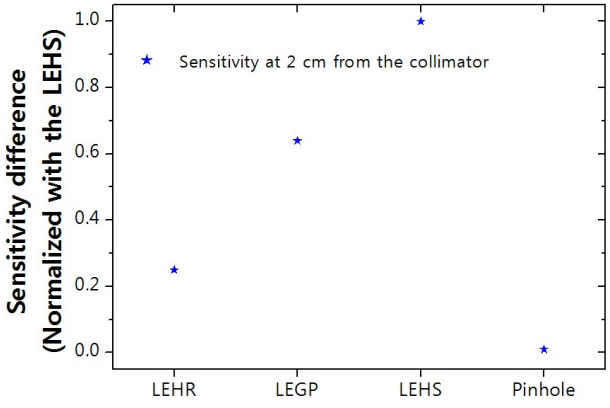

FIG. 5. Comparison of simulation results for the sensitivity at 2 cm source-to-collimator distance. The results are normalized with respect to the sensitivity obtained with a LEHS parallel-hole collimator.

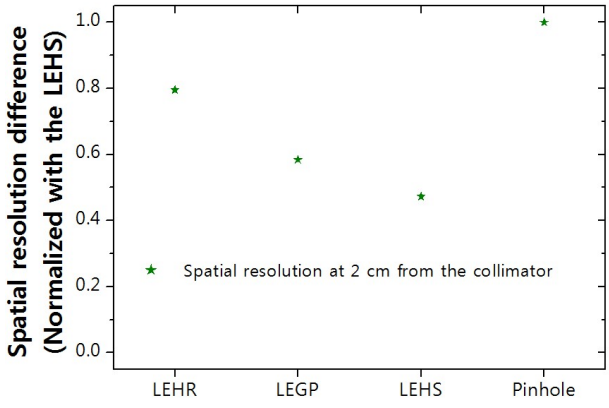

FIG. 7. Comparison of simulation results for the spatial resolution at 2 cm source-to-collimator distance. The results are normalized with respect to the spatial resolution obtained with a pinhole collimator.

or LEHR parallel-hole collimator was 2.0 mm or less at 2 cm source-to-collimator distance, while the other parallel-hole collimators provided about 3.0 mm.

Finally, reconstructed images of the simulated hot-rod phantoms for each source-to-collimator distance are shown in Fig. 8. The 2.0 mm rods were clearly resolved using the LEHR parallel-hole collimator at 1 and 2 cm from the collimator, or using the pinhole collimator. Additionally, overall imaging performance in the reconstructed hot-rod phantom images were in close agreement with the experimental average spatial resolutions.

Imaging performance, such as sensitivity and spatial resolution, is determined by a relationship between the direction of the detection point and the emitted gamma ray [25]. For a given total irradiation time, a high-sensitivity collimator such as an LEHScan acquire more counts, because this collimator has wide holes. However, it is increasingly realized that the quality of the counts is important, so the recommendation is generally against using a high-sensitivity collimator in this situation. Thus, the choice of high-resolution collimator, such as an LEHR parallel-hole or pinhole collimator, is against using a high-sensitivity collimator. The use of a highresolution collimator is recommended for a gamma-camera system, unless conditions suggest that unacceptably low count levels would occur. Consequently, the trade-off between sensitivity and spatial resolution remains a fundamental consideration for the type of collimator to obtain optimal imaging performance. The results of this study will be especially helpful in choosing a collimator in different situations.

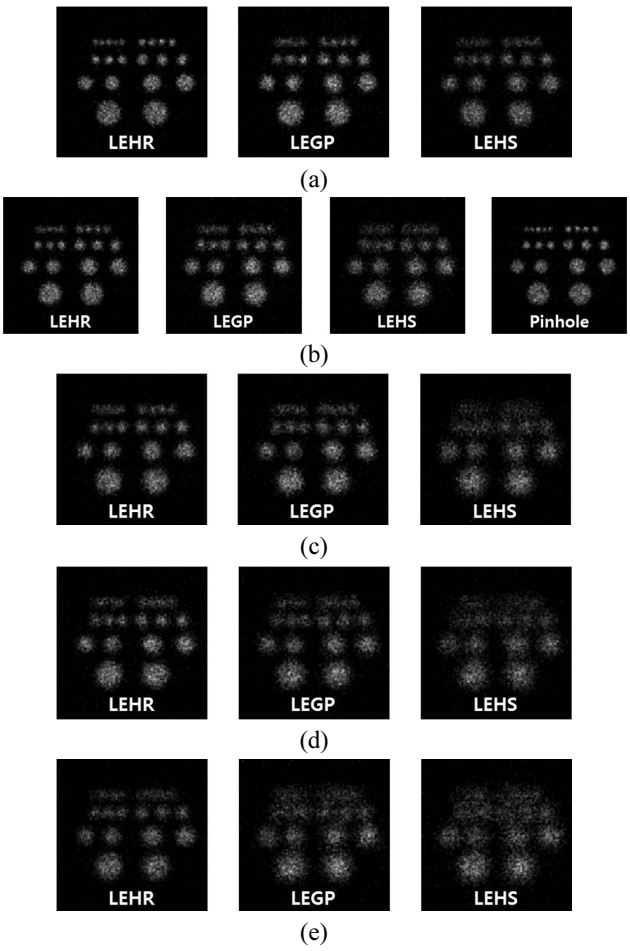

FIG. 8. Reconstructed images of the hot-rod phantom for a pinhole collimator and three parallel-hole collimators, for source-to-collimator distance of (a) 1, (b) 2, (c) 3, (d) 4, and (e) 5 cm.

IV. CONCLUSION

In the field of nuclear medicine, we recommend applying a PSD to improve both sensitivity and spatial resolution. A collimator study with a preclinical PSD by means of GATE simulation has been performed. We have presented a comparison of results for pinhole, LEHR parallel-hole, LEGP parallel-hole, and LEHS parallel-hole collimators in a preclinical pixelated semiconductor SPECT system. We also evaluated and compared the abovementioned collimators.

This study offers information for the choice of appropriate collimators for various purposes. According to the results, although parallel-hole collimators are often used in preclinical imaging, a pinhole collimator should be used to obtain images with high spatial resolution. Based on these results, we need to consider various types of collimators to obtain higher performance from the imaging system.

ACKNOWLEDGMENT

This work was partly supported by the Bio-Meditech Regional Innovation Center at Eulji University, under the Regional Innovation Center Program (2016-02-05) of the Ministry Of Trade, Industry and Energy.

REFERENCES

1. H. O. Anger, "Scintillation camera with multichannel collimators," J. Nucl. Ned. **5**, 515-531 (1964).
2. H. Wieczorek and A. Goedicke, "Analytical model for SPECT detector concepts," IEEE Trnas. Nucl. Sci. **53**, 1102-1112 (2006).
3. C. Scheiber and G. C. Giakos, "Medical applications of CdTe and CdZnTe detectors," Nucl. Instrum. Meth. Phys. Res. **458**, 12-25 (2001).
4. Y.-J. Lee, S.-J. Park, S.-W. Lee, D.-H. Kim, Y.-S. Kim, and H.-J. Kim, "Comparison of photon counting and conventional scintillation detectors in a pinhole SPECT system for small animal imaging: Monte Carlo simulation studies," J. Kor. Phys. Soc. **62**, 1317-1322 (2013).
5. Y.-J. Lee, H.-J. Ryu, S.-W. Lee, S.-J. Park, and H.-J. Kim, "Comparison of ultra-high-resolution parallel-hole collimator materials based on the CdTe pixelated semiconductor SPECT system," Nucl. Instrum. Meth. Phys. Res. **713**, 33-39 (2013).
6. T. Onodera, K. Hitomi, T. Shoji, and Y. Hiratate, "Pixellated

thallium bromide detectors for gamma-ray spectroscopy and imaging," Nucl. Instrum. Meth. Phys. Res. **525**, 199-204 (2004).
7. T. E. Peterson and L. R. Furenlid, "SPECT detectors: the Anger camera and beyond," Phys. Med. Biol. **56**, R145-R182 (2011).
8. S. C. Moore, K. Kouris, and I. Cullum, "Collimator design for single photon emission tomography," Eur. J. Nucl. Med. **19**, 138-150 (1992).
9. K. Ishizu, T. Mukai, Y. Yonekura, M. Pagani, T. Fujita, Y. Magata, S. Nishizawa, N. Tamaki, H. Shibasaki, and J. Konishi, "Ultra-high resolution SPECT system using four pinhole collimators for small animal studies," J. Nucl. Med. **36**, 2282-2287 (1995).
10. F. J. Beekman and B. Vastenhouw, "Design and simulation of a high-resolution stationary SPECT system for small animals," Phys. Med. Biol. **49**, 4579-4592 (2004).
11. H. Iida and K. Ogawa, "Comparison of a pixelated semiconductor detector and a non-pixelated scintillation detector in pinhole SPECT system for small animal study," Ann. Nucl. Med. **25**, 143-150 (2011).
12. R. J. Jaszczak, J. Li, H. Wang, M. R. Zalutsky, and R. E. Goleman, "Pinhole collimation for ultra-high-resolution, small-field-of-view SPECT," Phys. Med. Biol. **39**, 425-437 (1994).
13. K. Ogawa, T. Kawade, K. Nakamura, A. Kubo, and T. Ichihara, "Ultra high resolution pinhole SPECT for small animal study," IEEE Trnas. Nucl. Sci. **45**, 3122-3126 (1998).
14. S. Jan, D. Benoit, E. Becheva, T. Carlier, F. Cassol, P. Descourt, T. Frisson, L. Grevillot, L. Guigues, L. Maigne, C. Morel, Y. Perrot, N. Rehfeld, D. Sarrut, D. R. Schaart, S. Stute, U. Pietrzyk, D. Visvikis, N. Zahra, and I. Buvat, "GATE V6: a major enhancement of the GATE simulation platform enabling modelling of CT and radiotherapy," Phys. Med. Biol. **56**, 881-901 (2011).
15. A. Konik, M. T. Madsen, and J. J. Sunderland, "GATE simulations of small animal SPECT for determination of scatter fraction as a function of object size," IEEE Trnas. Nucl. Sci. **59**, 1887-1891 (2012).
16. S. Stute, T. Carlier, K. Cristina, C. Noblet, A. Martineau, B. Hutton, L. Barnden, and I. Buvat, "Monte Carlo simulations of clinical PET and SPECT scans: impact of the input data on the simulated images," Phys. Med. Biol. **56**, 6441-6457 (2011).
17. D. Lazaro, I. Buvat, G. Loudos, D. Strul, G. Santin, N. Giokaris, D. Donnarieix, L. Maigne, V. Spanoudaki, S. Styliaris, S. Staelens, and V. Breton, "Validation of the GATE Monte Carlo simulation platform for modelling a CsI(Tl) scintillation camera dedicated to small-animal imaging," Phys. Med. Biol. **49**, 271-285 (2004).
18. D. Bollini, A. E. Cabal Rodriguez, W. Dabrowski, A. D. Garcia, M. Gambaccini, P. Giubellino, P. Grybos, M. Idzik, A. Marzari-Chiesa, L. M. Montano, F. Prino, L. Ramello, M. Sitta, K. Swientek, R. Wheadon, and P. Wiacek, "Energy resolution of a silicon detector with the RX64 ASIC designed for X-ray imaging," Nucl. Instrum. Meth. Phys. Res. **515**, 458-466 (2003).
19. M. Singh and C. Horne, "Use of a germanium detector to optimize scatter correction in SPECT," J. Nucl. Med. **28**, 1853-1860 (1987).
20. T. Takahashi and S. Watanabe, "Recent progress in CdTe and CdZnTe detectors," IEEE Trans. Nucl. Sci. **48**, 950-959 (2001).
21. J. Xu, S. Miyazaki, and M. Hirose, "High-quality hydrogenated amorphous silicon-germanium alloys for narrow bandgap thin film solar cells," J. Non-Crys. Solids **208**, 277-281 (1996).
22. S. D. Sordo, L. Abbene, E. Caroli, A. M. Mancini, A. Zappettini, and P. Ubertini, "Progress in the development of CdTe and CdZnTe semiconductor radiation detectors for astrophysical and medical applications," Sensors **9**, 3491-3526 (2009).
23. C. Scheiber, "CdTe and CdZnTe detectors in nuclear medicine," Nucl. Instrum. Meth. Phys. Res. **448**, 513-524 (2000).
24. H. Toyokawa, Y. Furukawa, T. Hirono, H. Ikeda, K. Kajiwara, M. Kawase, T. Ohata, G. Sato, M. Sato, T. Takahashi, H. Tanida, T. Uruga, and S. Watanabe, "Si and CdTe pixel detector developments at Spring-8," Nucl. Instrum. Meth. Phys. Res. **636**, S218-S221 (2011).
25. Y.-J. Lee and H.-J. Kim, "Comparison of a newly-designed stack-up collimator with conventional parallel-hole collimators in pre-clinical CZT gamma camera systems: a Monte Carlo simulation study," J. Kor. Phys. Soc. **65**, 1149-1158 (2014).